


Cite this: *RSC Adv.*, 2023, **13**, 16067

Received 3rd March 2023

Accepted 1st May 2023

DOI: 10.1039/d3ra01438j

rsc.li/rsc-advances

# Graphene oxide supported ionic liquid/Fe complex: a robust and highly stable nanocatalyst

Kimiya Taheri, Dawood Elhamifar, \* Shiva Kargar  and Ali Zarnegaryan

Herein, a lamellar structured nano-graphene oxide supported ionic liquid/Fe complex (NGO/IL–Fe) is prepared through grafting of alkyl imidazolium chloride on the NGO followed by treatment with iron(III) chloride hexahydrate. The NGO/IL–Fe nanomaterial was characterized by using FT-IR, PXRD, TGA, EDX and SEM techniques. NGO/IL–Fe was used as a robust and efficient nanocatalyst for the synthesis of tetrahydrobenzo[*b*]pyrans in water at 25 °C. The desired products were obtained in high yield over a relatively short time. The recoverability, reusability and also leaching tests were performed to study the stability and the nature of the designed catalyst under applied conditions.

## 1. Introduction

Carbon-based nanomaterials have tremendously impacted numerous research fields such as drug delivery, adsorption, biomedical imaging, sensing and environmental remediation, owing to their unique properties and relatively simple preparation. In particular, graphene nanosheets have been the major focus of recent research as a unique 2D material with higher thermal and electrical conductivities, better mechanical strength, and larger specific surface area ( $>2600 \text{ m}^2 \text{ g}^{-1}$ ), in comparison to other carbon materials.<sup>1–7</sup> These unique features make graphene extremely attractive as a 2D catalyst support. However, the tendency of graphene sheets to aggregate through strong van der Waals forces would hinder their practical application. Graphene oxide (GO) with numerous surface oxygen-containing functional groups not only effectively overcomes the limitations of graphene nanosheets, but also possesses more active sites for interaction with catalytically-active species. GO has also the great advantages of low cost, easy preparation and good dispersibility in both aqueous and organic media.<sup>8–14</sup> Some of the recently developed reports of GO in the catalytic world are GO–Al500,<sup>10</sup> GO–PEG–imidazole–Pd (NHC)<sup>+</sup>,<sup>15</sup> Cu(salen)–*f*–GO,<sup>16</sup> GO–Cs<sub>2</sub>Mo<sub>6</sub>Br<sub>8</sub>Br<sub>6</sub>,<sup>17</sup> CuO–GO–TiO<sub>2</sub>,<sup>18</sup> GOCNT–Pt,<sup>19</sup> GO–Cu–AA,<sup>20</sup> and Cu<sub>2</sub>O/PPy–GO.<sup>21</sup> However, some of these catalytic systems suffer from drawbacks of instability and leaching of the transition metal (TM) complexes during reaction process. These drawbacks may be attributed to the weak interaction between TM complexes and the GO support as well as the aggregation of the metal NPs on the surface of the material. Therefore, developing efficient GO supported catalytic systems with high activity and stability still remains a great challenge in catalysis field.

Meanwhile, ionic liquids (IL) due to their tunable hydrophobicity, high conductivity, negligible vapor pressure, high chemical stability, and ionic and polar properties have attracted extensive attention as remarkable stabilizers to prevent aggregation of TM complexes in catalytic transformations.<sup>13,22–24</sup>

On the other hand, due to the biological activity of tetrahydrobenzo[*b*]pyrans such as anticancer, antispasmodic, anti-anaphylactic and anticoagulant, the development of efficient methods for their preparation is an extremely important subject between chemists. To date, tetrahydrobenzo[*b*]pyrans have been prepared through several developed methods.<sup>25–28</sup> However, various limitations are associated with these methods, such as high catalyst loading, low yields, the use of expensive ligands, tedious work-ups, difficult separation of product and catalyst, and the use of hazardous solvents. Thus, it is highly required to develop an environmentally-friendly, highly efficient, simple and affordable method for the synthesis of tetrahydrobenzo[*b*]pyrans.

In view of the above, in this work, we report the synthesis of a novel nano-graphene oxide/ionic liquid material supported Fe complex (NGO/IL–Fe) as well as its catalytic performance in the green preparation of tetrahydrobenzo[*b*]pyrans.

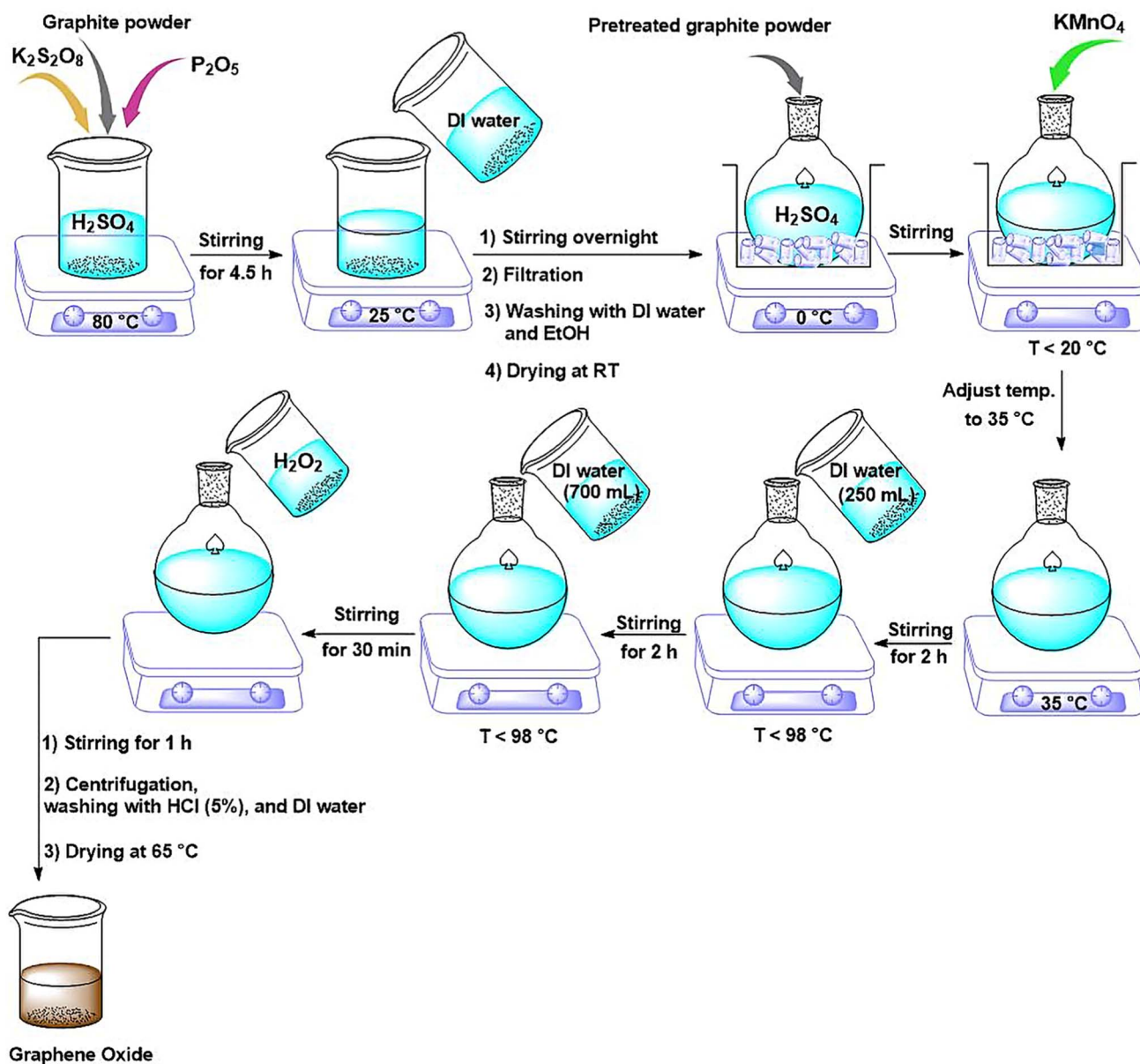
## 2. Experimental section

### 2.1. Materials and instrumentation

Graphite powder, 1-methylimidazole (99%), (3-chloropropyl)-trimethoxysilane (97%), iron(III) chloride hexahydrate ( $\geq 99\%$ ), dimedone (95%), malononitrile ( $\geq 99\%$ ), and ethanol (99%) were all purchased from Sigma-Aldrich. Sulfuric acid (95–98%), phosphorus pentoxide, potassium persulfate, potassium permanganate, hydrogen peroxide (30%), hydrochloric acid (37%), and benzaldehydes (97–99%) were purchased from Merck. Deionized water was distilled by water purification system (Milli-Q System). Fourier transform infrared (FT-IR)

Department of Chemistry, Yasouj University, Yasouj, 75918-74831, Iran. E-mail: d.elhamifar@yu.ac.ir





Scheme 1 Synthesis of nano-graphene oxide using modified Hummers' method.

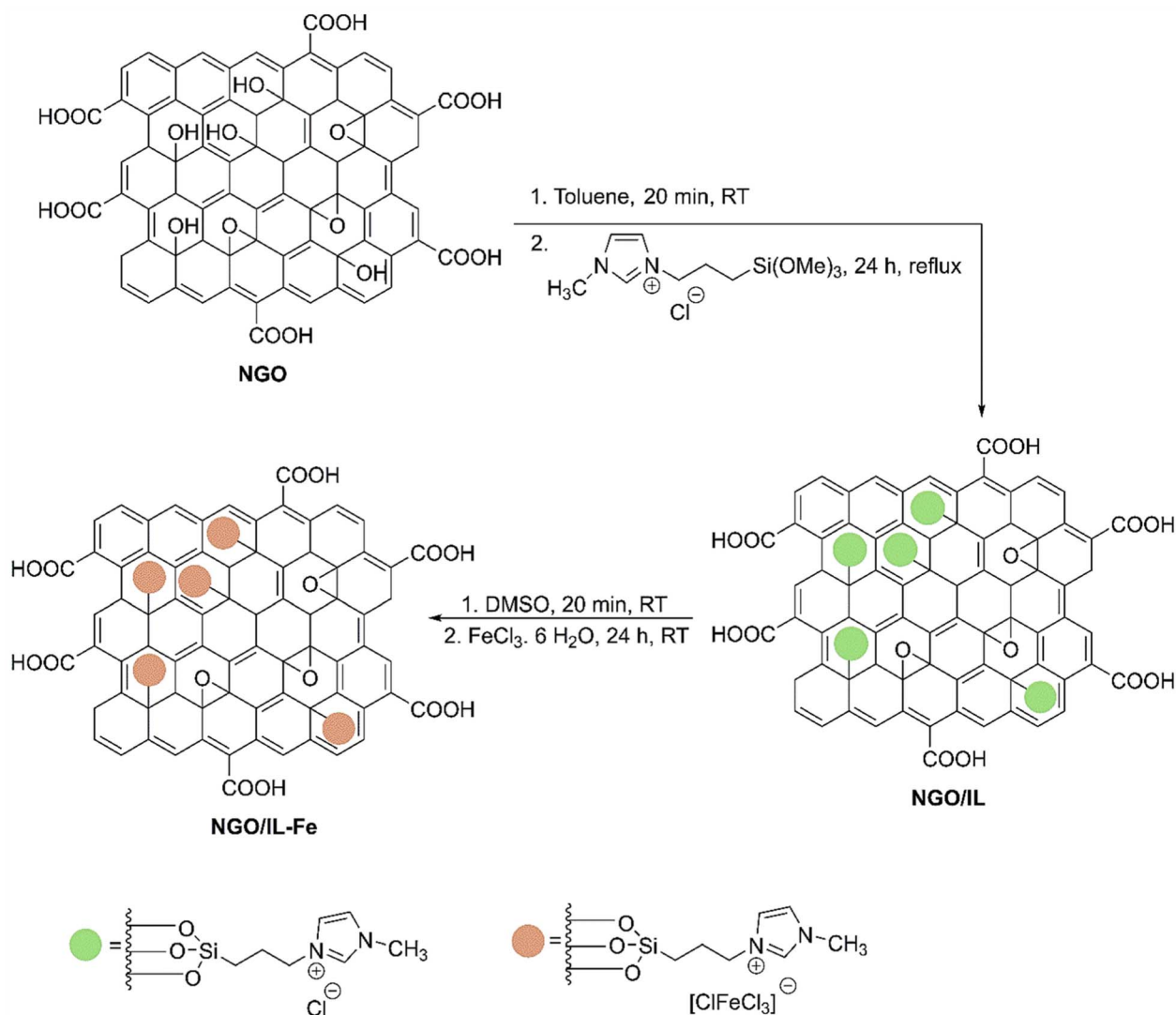
spectroscopy was recorded on a Bruker-Vector 22 spectrometer (Germany). Powder X-ray diffraction (PXRD) was obtained using a Bruker D8 ADVANCE diffractometer (Germany). Thermal gravimetric analysis (TGA) was carried out using a Netzsch STA 409 PC/PG apparatus (Germany). The morphology of the particles was characterized by TESCAN-Vega 3 scanning electron microscope (SEM) (Czech Republic). Energy dispersive X-ray (EDX) spectroscopy was obtained by using TESCAN-Vega 3 apparatus (Czech Republic).

## 2.2. Synthesis of nano-graphene oxide (NGO)

NGO was prepared according to the modified Hummers' method.<sup>29</sup> Typically, 3 g of graphite powder was added to a solution of concentrated  $H_2SO_4$  (12 mL),  $K_2S_2O_8$  (2.5 g) and  $P_2O_5$  (2.5 g). The resulted mixture was stirred at  $80\text{ }^\circ\text{C}$  for 4.5 h.

The solution was then cooled to room temperature, diluted with 500 mL of deionized water and left to stir overnight. Afterwards, the mixture was filtered and washed with distilled water and ethanol, and dried at room temperature for 12 h. Next, the collected powder was added to a round-bottom flask placed in an ice bath containing  $H_2SO_4$  (120 mL). While vigorously stirring, 15 mg of  $KMnO_4$  was gradually added to the suspension and the temperature was controlled below  $20\text{ }^\circ\text{C}$ . The solution was then stirred at  $35\text{ }^\circ\text{C}$  for 2 h. Next, the deionized water (250 mL) was added to the reaction vessel and stirred for another 2 h, while the temperature was controlled below  $98\text{ }^\circ\text{C}$ . Then, an additional distilled water (700 mL) was added and the resulted mixture was stirred for 30 min. Subsequently, 20 mL of  $H_2O_2$  (30%) was added while stirring was continued for 1 h. Finally, the suspension was repeatedly centrifuged, washed with HCl





Scheme 2 Preparation of the NGO/IL-Fe nanocatalyst.

solution (5%) and deionized water until a neutral pH was reached. The product was dried at 65 °C for 4 h in a vacuum oven and called NGO.

### 2.3. Synthesis of GO/IL nanocomposite (NGO/IL)

To synthesize of NGO/IL, ultrasonic irradiation was firstly used to disperse the as-prepared NGO (1 g) in toluene (35 mL). After adding 60 mg of 1-methyl-3-(3-trimethoxysilylpropyl)-imidazolium chloride (IL), the mixture was being reflux for 24 hours. The resulted material was filtered, completely washed with EtOH and dried at 70 °C to give NGO/IL.

### 2.4. Synthesis of NGO/IL-Fe

For this, firstly, NGO/IL (1 g) and dimethyl sulfoxide (35 mL) were added to a reaction vessel and sonicated at RT for 10 min. Then,  $\text{FeCl}_3 \cdot 6\text{H}_2\text{O}$  (4 mmol) was added to the obtained suspension while stirring at RT for 24 h. Eventually, the resulted

mixture was filtered and the product was washed with EtOH completely, dried at 70 °C for 6 h and denoted as NGO/IL-Fe.

### 2.5. Procedure for the preparation of tetrahydrobenzo[b]pyrans using NGO/IL-Fe

For this, NGO/IL-Fe (0.08 mol%), benzaldehyde (1 mmol), malononitrile (1.3 mmol) and dimedone (1 mmol) were added in  $\text{H}_2\text{O}$  (5 mL) while stirring at RT. Upon completion of the reaction (monitored by TLC), the NGO/IL-Fe catalyst was removed by filtration using a filter paper. Finally, hot EtOH was added and the resulted mixture was put in an ice bath to precipitate/crystallize the pure product. The obtained products were characterized by using IR and NMR techniques.

### 2.6. IR, $^1\text{H}$ NMR and $^{13}\text{C}$ NMR data of tetrahydrobenzo[b]pyrans

**2.6.1. 2-Amino-4-(4-methoxyphenyl)-7,7-dimethyl-5-oxo-6,6,8,8-tetrahydro-4H-chromene-3-carbonitrile.** White solid;

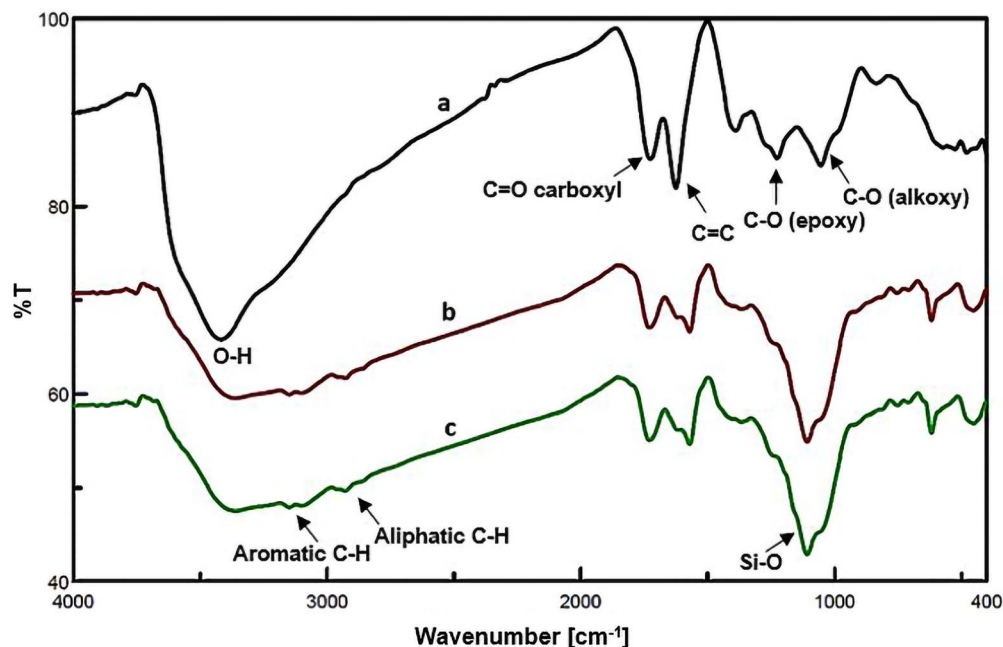


Fig. 1 FT-IR spectra of GO (a), NGO/IL (b) and NGO/IL-Fe (c).

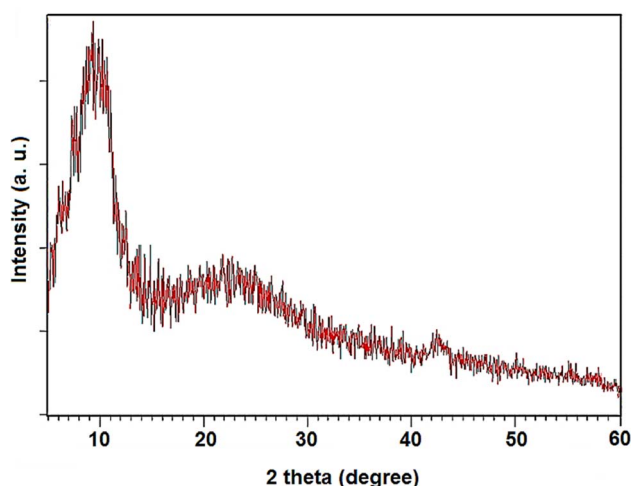


Fig. 2 XRD patterns of NGO/IL-Fe.

mp: 198–200 °C (196–198).<sup>30</sup> IR (KBr,  $\text{cm}^{-1}$ ): 3425, 3347 ( $\text{NH}_2$ , stretching vibration), 3097 ( $=\text{C}-\text{H}$ , stretching vibration  $\text{sp}^2$ ), 2964 ( $\text{C}-\text{H}$ , stretching vibration  $\text{sp}^3$ ), 2189 ( $\text{CN}$ , stretching vibration), 1673 ( $\text{C}=\text{O}$ , stretching vibration), 1552, 1411 ( $\text{C}=\text{C}$ , Ar stretching vibration  $\text{sp}^2$ ), 1243 ( $\text{C}-\text{O}$ , stretching vibration).  $^1\text{H}$  NMR (300 MHz,  $\text{CDCl}_3$ ):  $\delta$  (ppm) 1.02 (s, 3H), 1.10 (s, 3H), 2.18 (d, 1H,  $J = 3.6$  Hz), 2.20 (d, 1H,  $J = 3.3$  Hz), 2.43 (s, 2H), 3.76 (s, 3H), 4.35 (s, 1H), 4.51 (s, 2H,  $\text{NH}_2$ ), 6.79 (d, 2H,  $J = 8.6$  Hz), 7.13 (d, 2H,  $J = 8.6$  Hz).  $^{13}\text{C}$  NMR (75 MHz,  $\text{CDCl}_3$ ):  $\delta$  (ppm) 27.6, 28.8, 32.2, 34.7, 40.6, 50.7, 55.2, 63.9, 113.9, 114.2, 115.1, 128.6, 133.4, 135.4, 157.3, 158.6, 161.2, 195.9.

**2.6.2. 2-Amino-4-(4-methylphenyl)-7,7-dimethyl-5-oxo-6,6,8,8-tetrahydro-4H-chromene-3-carbonitrile.** White solid; mp: 216–218 °C (220–222).<sup>30</sup> IR (KBr,  $\text{cm}^{-1}$ ): 3423, 3325 ( $\text{NH}_2$ ,

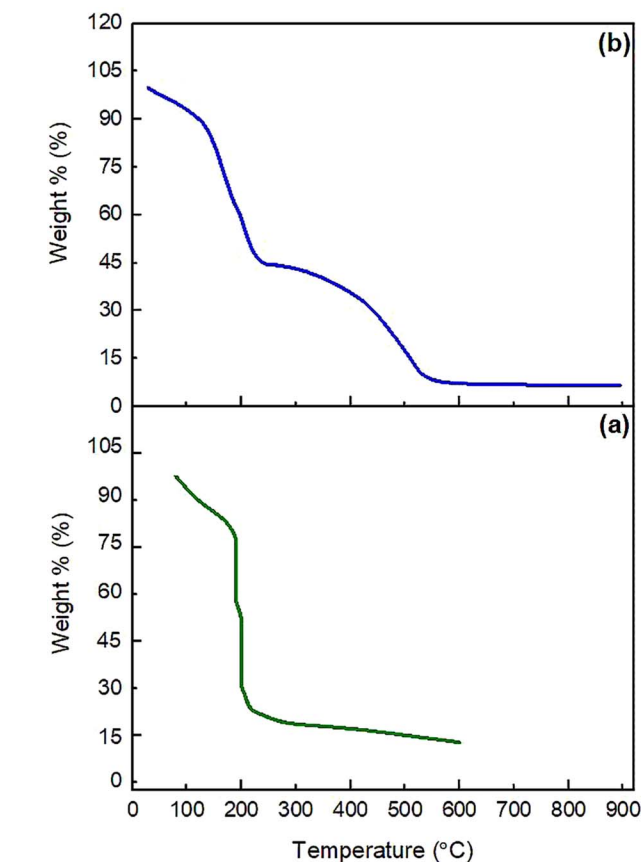


Fig. 3 TG curves of GO (a), and NGO/IL-Fe nanocatalyst (b).

stretching vibration), 3048 ( $=\text{C}-\text{H}$ , stretching vibration  $\text{sp}^2$ ), 2958 ( $\text{C}-\text{H}$ , stretching vibration  $\text{sp}^3$ ), 2191 ( $\text{CN}$ , stretching vibration), 1671 ( $\text{C}=\text{O}$ , stretching vibration), 1565, 1482 ( $\text{C}=\text{C}$ ,





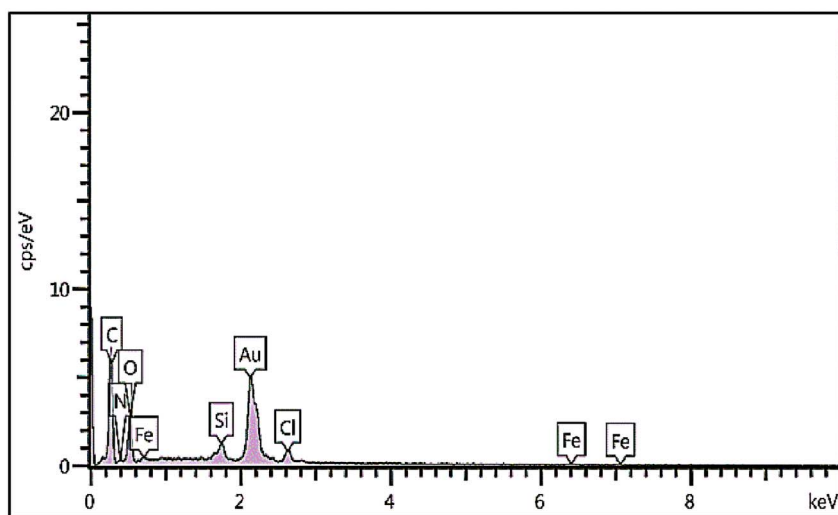


Fig. 4 EDX spectrum of NGO/IL-Fe.

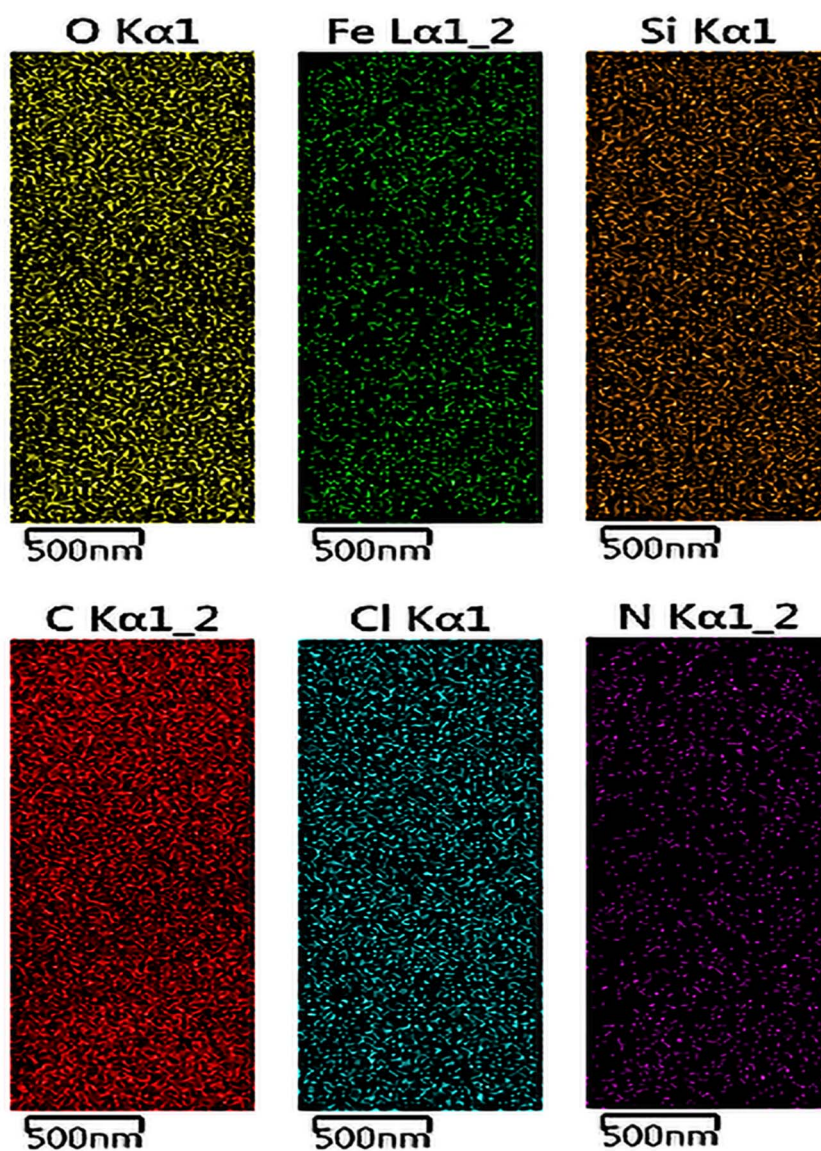


Fig. 5 EDX-mapping of NGO/IL-Fe.



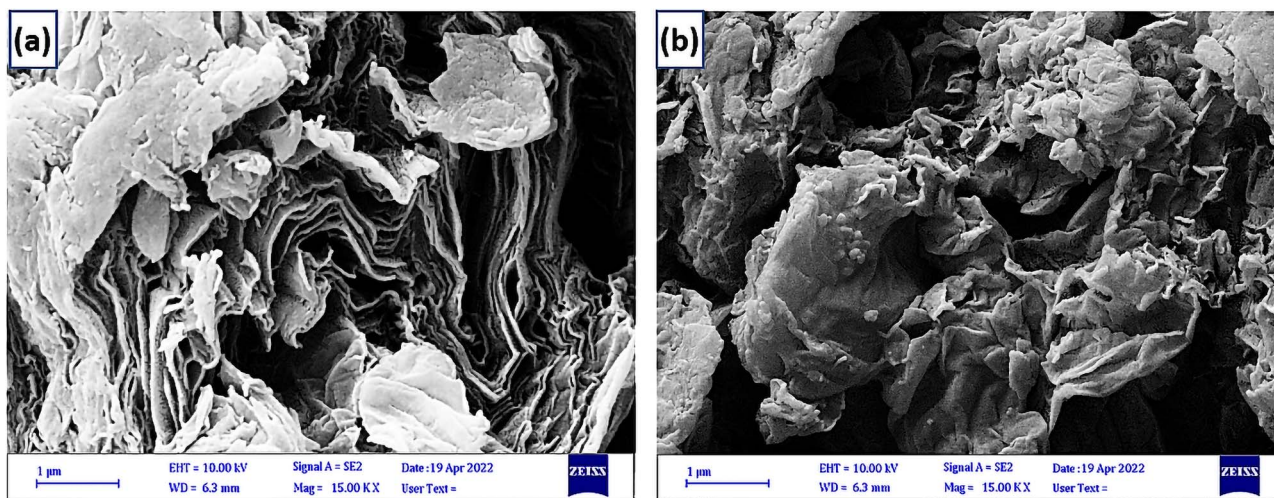


Fig. 6 SEM images of GO (a) and NGO/IL-Fe (b).

Table 1 Synthesis of tetrahydrobenzo[b]pyrans under different conditions

Entry	Solvent	Catalyst	Catalyst loading (mol%)	Time (min)	Yield (%)
1	EtOH	NGO/IL-Fe	0.08	45	78
2 <sup>a</sup>	H <sub>2</sub> O	NGO/IL-Fe	0.08	45	91
3	Solvent-free	NGO/IL-Fe	0.08	45	80
4	H <sub>2</sub> O	NGO/IL-Fe	0.04	45	65
5	H <sub>2</sub> O	Catalyst-free	—	120	—
6	H <sub>2</sub> O	NGO@Fe	0.01 (g)	45	75

<sup>a</sup> Optimized condition.

Ar stretching vibration  $\text{sp}^2$ ), 1246 (C–O, stretching vibration). <sup>1</sup>H NMR (300 MHz,  $\text{CDCl}_3$ ):  $\delta$  (ppm) 1.06 (s, 3H), 1.12 (s, 3H), 2.11 (d, 1H,  $J = 6.2$  Hz), 2.23 (d, 1H,  $J = 15.7$  Hz), 2.28 (s, 3H), 2.56 (s, 2H), 4.38 (s, 1H), 7.02–7.13 (m, 4H), 7.31 (s, 2H). <sup>13</sup>C NMR (75 MHz,  $\text{CDCl}_3$ ):  $\delta$  (ppm) 21.2, 27.6, 28.9, 32.7, 35.3, 40.8, 50.5, 63.9, 114.0, 118.5, 127.7, 129.2, 136.9, 139.8, 157.1, 159.8, 161.5, 196.2.

**2.6.3. 2-Amino-4-(3-nitrophenyl)-7,7-dimethyl-5-oxo-6,6,8,8-tetrahydro-4H-chromene-3-carbonitrile.** White solid; mp: 214–216 °C (214–216).<sup>30</sup> IR (KBr,  $\text{cm}^{-1}$ ): 3352, 3432 ( $\text{NH}_2$ , stretching vibration), 3152 ( $=\text{C}-\text{H}$ , stretching vibration  $\text{sp}^2$ ), 2953 (C–H, stretching vibration  $\text{sp}^3$ ), 2190 (CN, stretching vibration), 1667 (C=O, stretching vibration), 1531, 1468 (C=C, Ar stretching vibration  $\text{sp}^2$ ), 1256 (C–O, stretching vibration), 1531, 1416 ( $\text{NO}_2$  stretching vibration). <sup>1</sup>H NMR (300 MHz,  $\text{CDCl}_3$ ):  $\delta$  (ppm) 0.97 (s, 3H), 1.08 (s, 3H), 2.13 (d, 1H,  $J = 15$  Hz), 2.30 (d, 1H,  $J = 15$  Hz), 2.57 (s, 2H), 4.45 (s, 1H), 7.22 (s, 2H), 7.61–7.71 (m, 2H), 8.0 (s, 1H), 8.09 (d, 1H,  $J = 9$  Hz). <sup>13</sup>C NMR (75

MHz,  $\text{CDCl}_3$ ):  $\delta$  (ppm) 27.2, 28.8, 32.3, 35.8, 40.6, 50.3, 56.8, 57.6, 112.2, 119.8, 122.1, 122.2, 130.5, 134.6, 147.4, 148.2, 159.1, 163.6, 196.2.

## 3. Results and discussion

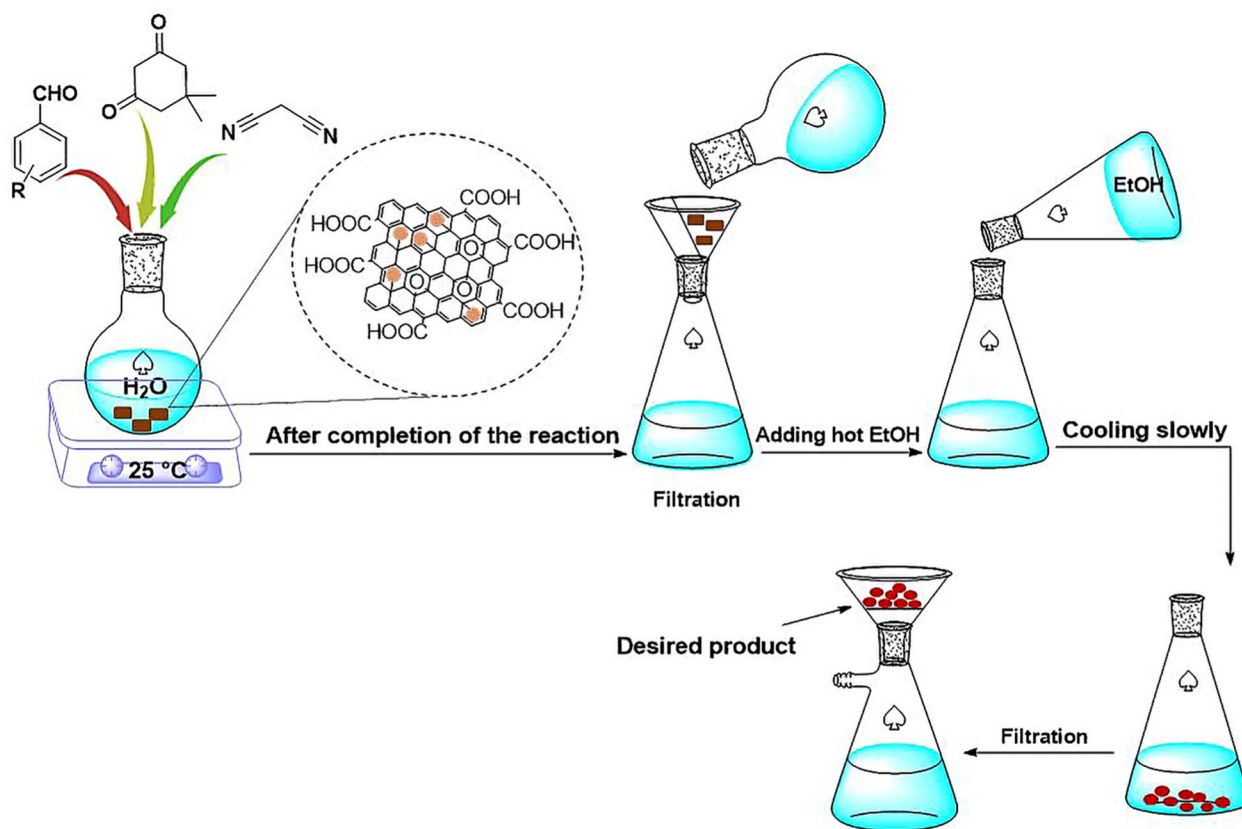
### 3.1. Synthesis and characterization of NGO/IL-Fe

Scheme 2 illustrates the synthesis procedure of NGO/IL-Fe nanocatalyst. First, NGO was synthesized according to the modified Hummers' method (Scheme 1).<sup>29</sup> Then, ionic liquid was chemically grafted on NGO to give NGO/IL material. Finally, the NGO/IL nanomaterial was treated with  $\text{FeCl}_3 \cdot 6\text{H}_2\text{O}$  to deliver the NGO/IL-Fe catalyst (Scheme 2).

The FT-IR was used to demonstrate the functional moieties of the designed nanocatalyst. As illustrated in Fig. 1, all samples display the peaks at 3424, 1723, 1623, 1226, and 1058  $\text{cm}^{-1}$ , which are attributed to the stretching vibrations of  $-\text{OH}$ ,  $\text{C}=\text{O}$ ,  $\text{C}=\text{C}$ , epoxy  $-\text{C}-\text{O}$ , and  $-\text{C}-\text{O}$  alkoxy bonds, respectively,







**Scheme 3** The schematic representation for the synthesis of tetrahydrobenzo[*b*]pyrans. Conditions: NGO/IL–Fe catalyst (0.08 mol%), aldehyde (1 mmol), dimedone (1 mmol), malononitrile (1.3 mmol), H<sub>2</sub>O solvent and 25 °C.

indicating the presence of oxygen-containing functional groups on the GO surface.<sup>31</sup> Also, the characteristic peaks of aromatic C–H, aliphatic C–H, and Si–O bonds, respectively, at 3151, 2919 and 1090 cm<sup>−1</sup> confirm that the ionic liquid groups are successfully grafted onto the surface of GO (Fig. 1b and c).<sup>32</sup>

The XRD pattern of NGO/IL–Fe is shown in Fig. 2. As illustrated, the well-defined peaks centered at 11.02° and 42.8° are attributed to the (001) and (100) crystalline planes of GO, respectively.<sup>33</sup> The broad peak at 24.3° is attributed to the successful immobilization of IL–Fe complex on the layer of GO.<sup>34</sup>

The thermal stability of GO and NGO/IL–Fe was investigated by thermal gravimetric analysis (TGA). As depicted in Fig. 3, GO displays two weight losses. The first one, below 110 °C (about 12%), is attributed to the loss of adsorbed water molecules.<sup>35</sup> The main weight loss (about 72%) occurred at 130–220 °C, corresponding to the pyrolysis of oxygen containing groups. Heating beyond 500 °C leads to the degradation of the carbon rings. The NGO/IL–Fe catalyst also shows a weight loss of around 12.5% below 110 °C due to the removal of water molecules. In the range of 130–220 °C, a weight loss of 44.5% is due to the decomposition of oxygen containing groups. This is significantly decreased compared to that of pristine GO, indicating that the thermal stability of GO is greatly improved after the immobilization of IL/Fe complex. In addition, the complete

decomposition of the IL moieties and GO skeleton (about 37%) is occurred between 230 and 670 °C. These results indicate that the IL moieties are successfully grafted onto the GO surface and also confirm the positive effect of immobilized ILs in the thermal stability of GO.

The immobilization of Fe on NGO/IL nanocomposite was also investigated by the EDX analysis (Fig. 4). This analysis clearly showed the presence of Fe, C, Cl, O, N and Si elements in the designed material proving the successful immobilization of Fe/IL complex on GO.

Moreover, the uniform distribution of the Fe, O, Cl, Si, N and C elements in the NGO/IL–Fe framework was well evidenced by the results obtained by the EDX-mapping analysis (Fig. 5). This is in good agreement with the FT-IR and TGA results.

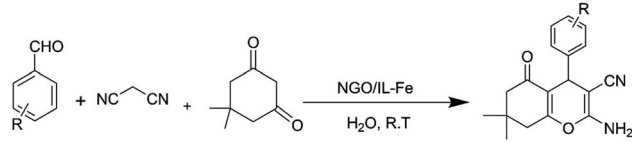
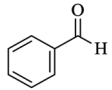
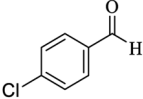
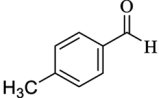
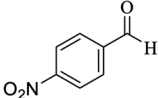
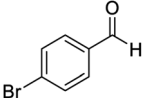
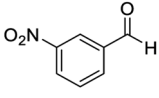
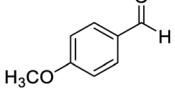
The scanning electron microscopy analysis presents the morphology of the GO and NGO/IL–Fe samples (Fig. 6). Compared with the flake-like shape of GO, the NGO/IL–Fe showed a sheet like structure with more crumpling features, confirming it has a high specific surface area and can be used as an extremely effective catalyst in organic reactions.

### 3.2. Catalytic activity of NGO/IL–Fe

After a comprehensive characterization of NGO/IL–Fe, its performance was studied in the synthesis of tetrahydrobenzo[*b*]pyrans. As a model reaction, the condensation between



Table 2 Synthesis of tetrahydrobenzo[b]pyrans catalyzed by NGO/IL-Fe

					
Entry	Aldehyde	Time (min)	Yield (%)	Found mp	Reported mp
1		45	91	229–231	228–230 (ref. 36)
2		35	92	212–214	210–212 (ref. 27)
3		50	90	218–220	220–222 (ref. 30)
4		25	92	177–179	179–181 (ref. 27)
5		30	93	204–206	203–205 (ref. 27)
6		30	89	214–216	214–216 (ref. 30)
7		75	89	198–200	196–198 (ref. 30)

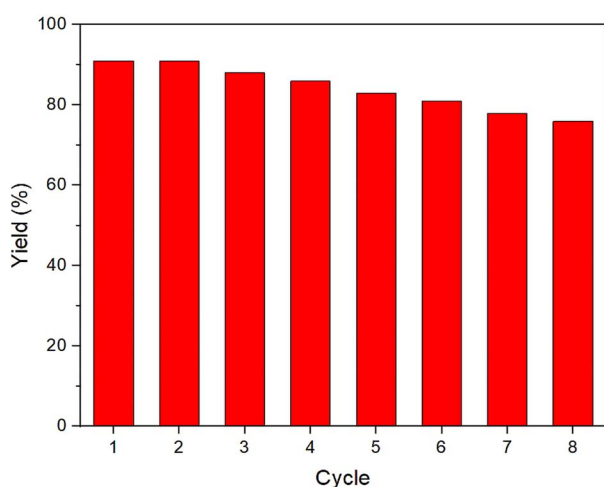


Fig. 7 Recoverability and reusability of the NGO/IL-Fe nanocatalyst.

dimedone, benzaldehyde and malononitrile at RT was chosen. The optimal conditions were determined by evaluating the effects of catalyst amount and solvent. The results revealed that

the highest yield (91%) is obtained in H<sub>2</sub>O compared to EtOH and solvent-free condition (Table 1, entry 2 vs. entries 1 and 3). The effect of catalyst loading was also evaluated and it was found that the use of 0.08 mol% of NGO/IL-Fe catalyst gives the highest product yield (Table 1, entry 2). It is also noteworthy that when the reaction was carried out without the NGO/IL-Fe catalyst, no product yield was obtained (Table 1, entry 5). These observations indicate that the presence of the NGO/IL-Fe catalyst is mandatory to catalyze this process. To elucidate the role of the imidazolium-based IL moiety, the reaction was also carried out in the presence of the IL-free NGO@Fe material (Table 1, entry 6). Attractively, the latter case showed significantly lower catalytic activity compared to the NGO/IL-Fe catalyst. It is also important to note, where the IL-free NGO@Fe material was used as catalyst, the Fe species were dramatically leached during the reaction progress confirming the key role of ILs in the immobilization and stabilization of Fe-catalytic centers. Therefore, the use of 0.08 mol% of NGO/IL-Fe catalyst, H<sub>2</sub>O solvent and 25 °C were selected as optimum conditions.

After determining the optimal conditions, the reaction was further carried out with a series of aldehydes containing either





electron-donating or electron-withdrawing substituents (Scheme 3). All aldehydes provided the desired products in high to excellent yields under applied conditions, indicating the high efficiency of the NGO/IL-Fe catalyst in the synthesis of a wide range of tetrahydrobenzo[*b*]pyrans (Table 2).

Considering the importance of the stability of the catalyst for its practical applications, in the next study, the recyclability of the designed NGO/IL-Fe nanocatalyst was examined. For this, upon completion of the reaction, the NGO/IL-Fe catalyst was separated and reused in the subsequent cycles under identical conditions as the first run. It was found that the NGO/IL-Fe catalyst retain its high activity for at least seven cycles, proving its outstanding durability under applied conditions (Fig. 7).

The nature of the NGO/IL-Fe nanocatalyst under the employed conditions was studied *via* a leaching experiment. To do this, the designed catalyst was removed at a conversion of about 50% and then the progress of the catalyst-free solution was studied for 120 min. Interestingly, no further conversion was observed, confirming no leaching of Fe species during reaction process and also the heterogeneous nature of the NGO/IL-Fe catalyst.

In the next, in order to study the chemical and structural stability of the catalyst under applied conditions, the EDX and SEM analyses were performed on the recycled catalyst. As shown in Fig. 8, no significant difference is observed in the EDX-pattern and element composition of the recovered catalyst after seven runs compared with those of the fresh NGO/IL-Fe catalyst. These results indicate the high stability of the catalyst after reusing and recovering several times.

The SEM image of the recovered catalyst after three times showed a morphology approximately the same as fresh catalyst confirming the high stability of the designed material structure under applied conditions (Fig. 9).

A plausible mechanism for the synthesis of tetrahydrobenzo[*b*]pyrans using NGO/IL-Fe catalyst is outlined in Scheme 4. At

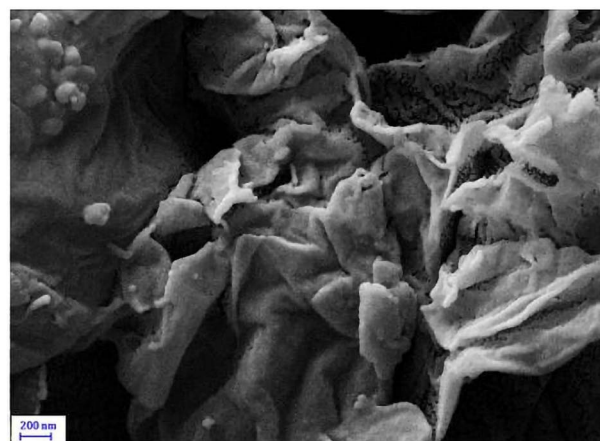


Fig. 9 SEM image of the recovered NGO/IL-Fe catalyst.

first, 2-arylidene malononitrile (**1**) is delivered through Knoevenagel condensation of the Fe-activated aldehyde with malononitrile. Intermediate **2** is then formed *via* Michael-type addition between intermediate **1** and the enol form of dime-done. Thereafter, intramolecular cyclization of intermediate **2** leads to the formation of intermediate **3**, which subsequently undergoes tautomerization to deliver the desired product **4** with a high yield. It is logical to deduce that imidazolium-based IL moiety plays a critical role on accelerating the reaction. In fact, ILs are spacers between GO support and catalytic Fe-species leading the catalytic sites more accessible. Moreover, owing to the ionic nature and polarity of ILs, they can effectively stabilize the catalytic active site by forming a strong electrostatic interaction between the imidazolium cation and [ClFeCl<sub>3</sub>] anion.<sup>37</sup>

In the next study, the performance of NGO/IL-Fe was compared to some previous catalytic systems that have been used in the in the synthesis of tetrahydrobenzo[*b*]pyrans (Table 3). The study indicated that our catalyst has more significant advantages

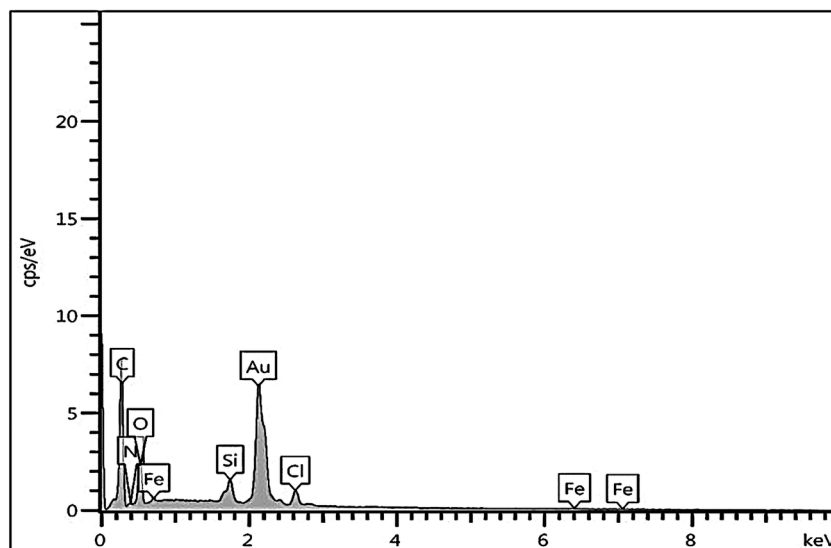
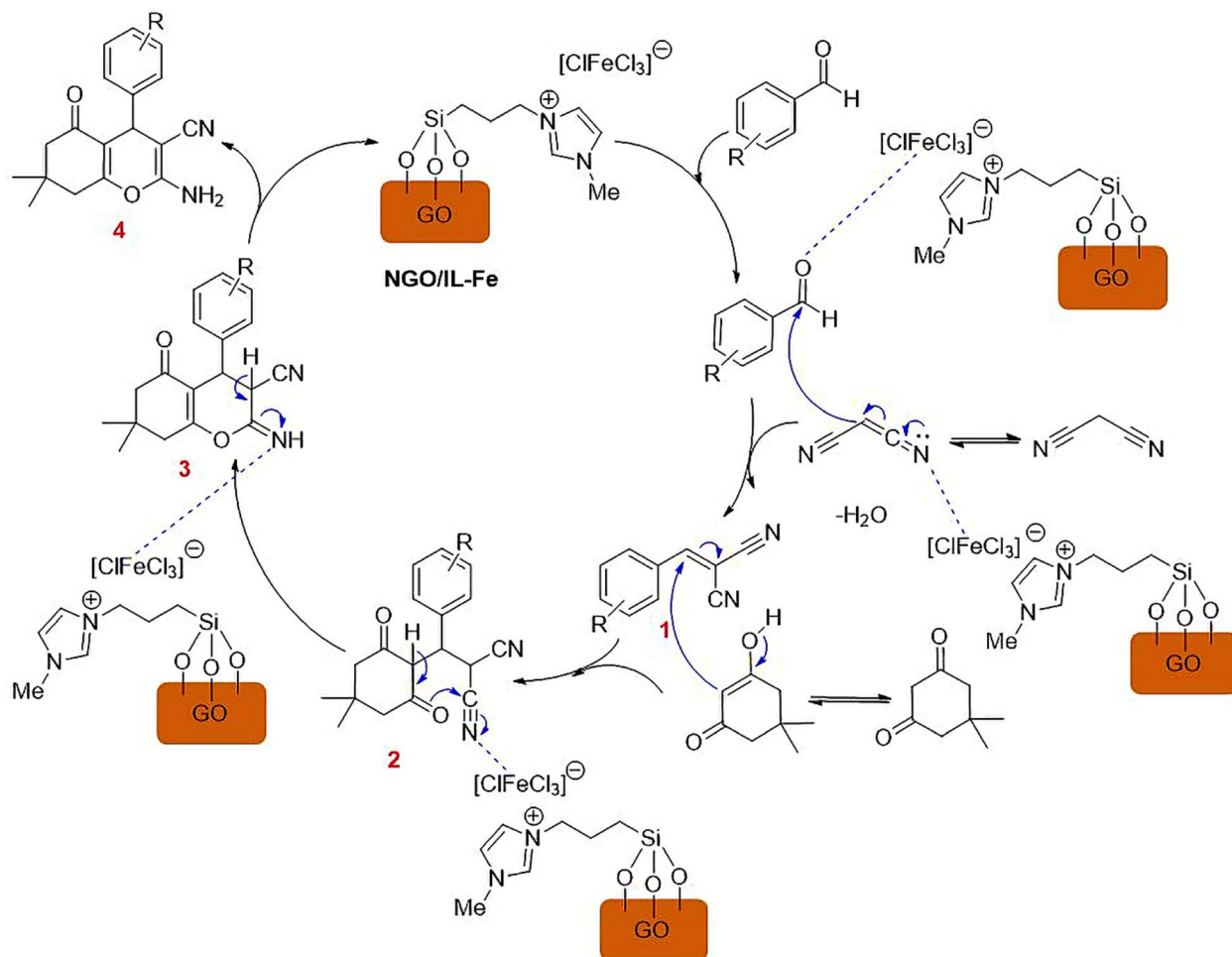


Fig. 8 EDX spectrum of the recovered NGO/IL-Fe nanocatalyst.



Scheme 4 A plausible mechanism for the synthesis of tetrahydrobenzo[*b*]pyrans using NGO/IL-Fe.

Table 3 Comparative study of the efficiency of NGO/IL-Fe with the former catalysts

Entry	Catalyst	Conditions	Yield (%)	Ref.
1	Fe <sub>3</sub> O <sub>4</sub> @SiO <sub>2</sub> @imid-PMA <sup>a</sup>	Cat. 0.02 g, H <sub>2</sub> O, reflux	82	38
2	Fe <sub>3</sub> O <sub>4</sub> @SiO <sub>2</sub> @TiO <sub>2</sub>	Cat. (0.01 g), solvent-free, 100 °C	75	39
3	Fe <sub>3</sub> O <sub>4</sub> @SiO <sub>2</sub> @NH-NH <sub>2</sub> -PW	Cat. (0.0.03 g), H <sub>2</sub> O, reflux	80	40
4	AIL@MNP	Cat. 60 mg, solvent-free, 90 °C	76	41
5	NGO/IL-Fe	Cat. 0.08 mol%, H <sub>2</sub> O, RT	91	This work

in the reaction temperature, catalyst loading and product yield. These finding may be attributed the key role of supported ILs in the stabilization of active catalytic Fe-centers.

## 4. Conclusion

In summary, in the present work, a novel nano-graphene oxide immobilized IL/Fe complex (NGO/IL-Fe) was successfully

designed and synthesized. The FT-IR, TG, and EDX analyses clearly indicated that the IL/Fe moieties are successfully immobilized on the NGO surface. These analyses also confirmed the high stability of the IL/Fe complex on NGO. The SEM image of NGO/IL-Fe demonstrated a well-defined sheet-like structure for this nanomaterial. The NGO/IL-Fe was effectively applied as a powerful nanocatalyst for the green synthesis of tetrahydrobenzo[*b*]pyrans in water as an environmentally-



friendly solvent. The NGO/IL-Fe catalyst was easily recovered, reused and kept its efficiency and stability after seven recycling times. Due to the aforementioned advantages of the designed NGO/IL-Fe catalyst, some of its applications in other chemical processes are underway in our laboratory.

## Conflicts of interest

There are no conflicts to declare.

## Acknowledgements

The authors thank Yasouj University and the Iran National Science Foundation (INSF) for supporting this work.

## References

- 1 T. Yang, S. Tang, X. Li, E. Sharman, J. Jiang and Y. Luo, *J. Phys. Chem. C*, 2018, **122**, 25441–25446.
- 2 N. Dong, Q. Ye, D. Zhang, Y. Xiao and H. Dai, *J. Hazard. Mater.*, 2022, **431**, 128518.
- 3 Y. Li, W. Gao, L. Ci, C. Wang and P. M. Ajayan, *Carbon*, 2010, **48**, 1124–1130.
- 4 P. V. Kamat, *J. Phys. Chem. Lett.*, 2010, **1**, 520–527.
- 5 V. Chabot, D. Higgins, A. Yu, X. Xiao, Z. Chen and J. Zhang, *Energy Environ. Sci.*, 2014, **7**, 1564–1596.
- 6 H. Burhan, K. Arikian, M. H. Alma, M. S. Nas, H. Karimi-Maleh, F. Şen, F. Karimi and Y. Vasseghian, *Int. J. Hydrogen Energy*, 2023, **48**, 6657–6665.
- 7 D. Zhou, B. Jiang, R. Yang, X. Hou and C. Zheng, *Chin. Chem. Lett.*, 2020, **31**, 1540–1544.
- 8 E. Antolini, *Appl. Catal., B*, 2012, **123**, 52–68.
- 9 M. E. Shabestari, O. Martín, D. Díaz-García, S. Gómez-Ruiz, V. J. Gonzalez and J. Baselga, *Carbon*, 2020, **161**, 7–16.
- 10 K. Iris, X. Xiong, D. C. Tsang, Y. H. Ng, J. H. Clark, J. Fan, S. Zhang, C. Hu and Y. S. Ok, *Green Chem.*, 2019, **21**, 4341–4353.
- 11 C. Prasad, Q. Liu, H. Tang, G. Yuvaraja, J. Long, A. Rammohan and G. V. Zyryanov, *J. Mol. Liq.*, 2020, **297**, 111826.
- 12 K. Zhang, K. Hong, J. M. Suh, T. H. Lee, O. Kwon, M. Shokouhimehr and H. W. Jang, *Res. Chem. Intermed.*, 2019, **45**, 599–611.
- 13 S. Kargar, D. Elhamifar and A. Zarnegaryan, *Surf. Interfaces*, 2021, **23**, 100946.
- 14 A. Zarnegaryan, Z. Dehbanipour and D. Elhamifar, *Polyhedron*, 2019, **170**, 530–536.
- 15 M. M. Heravi, S. Asadi, S. M. Hoseini Chopani and E. Jaderi, *Appl. Organomet. Chem.*, 2020, **34**, e5805.
- 16 Q. Zhao, C. Bai, W. Zhang, Y. Li, G. Zhang, F. Zhang and X. Fan, *Ind. Eng. Chem. Res.*, 2014, **53**, 4232–4238.
- 17 S. Kumar, O. P. Khatri, S. Cordier, R. Boukherroub and S. L. Jain, *Chem.-Eur. J.*, 2015, **21**, 3488–3494.
- 18 J. Zhao, D. C. T. Nguyen, Y. Areerob and W.-C. Oh, *Solid State Sci.*, 2019, **91**, 77–88.
- 19 H. Wang, S. Li, Y. Si, N. Zhang, Z. Sun, H. Wu and Y. Lin, *Nanoscale*, 2014, **6**, 8107–8116.
- 20 S. Mallakpour, A. Abdolmaleki and A. Karshenas, *Catal. Commun.*, 2017, **92**, 109–113.
- 21 P. Pattanayak, N. Pramanik, P. Kumar and P. P. Kundu, *Int. J. Hydrogen Energy*, 2018, **43**, 11505–11519.
- 22 S. Ding, M. J. Hülsey, H. An, Q. He, H. Asakura, M. Gao, J.-y. Hasegawa, T. Tanaka and N. Yan, *CCS Chem.*, 2021, **3**, 1814–1822.
- 23 M. M. Seitkalieva, D. E. Samoylenko, K. A. Lotsman, K. S. Rodygin and V. P. Ananikov, *Coord. Chem. Rev.*, 2021, **445**, 213982.
- 24 S. Rezayati, E. R. Nezhad and R. Hajinasiri, *Chin. Chem. Lett.*, 2016, **27**, 974–978.
- 25 P. Gupta, S. Rani, D. Sah, J. Shabir, B. Singh, B. Pani and S. Mozumdar, *J. Mol. Struct.*, 2023, **1274**, 134351.
- 26 C. Bouregghda, I. Amine Khodja, B. Carboni, R. Boulcina, O. Kermiche and A. Debache, *Lett. Org. Chem.*, 2016, **13**, 482–490.
- 27 M. Biglari, F. Shirini, N. O. Mahmoodi, M. Zabihzadeh and M. Mashhadinezhad, *J. Mol. Struct.*, 2020, **1205**, 127652.
- 28 Y. L. Hu, J. R. Li, C. Chen, X. B. Liu and Q. Rong, *Sustainable Chem. Pharm.*, 2022, **29**, 100779.
- 29 J.-M. Yan, Z.-L. Wang, H.-L. Wang and Q. Jiang, *J. Mater. Chem.*, 2012, **22**, 10990–10993.
- 30 K. S. Pandit, P. V. Chavan, U. V. Desai, M. A. Kulkarni and P. P. Wadgaonkar, *New J. Chem.*, 2015, **39**, 4452–4463.
- 31 Y. Liu, H. Du, Y. Meng, S. Lu, J. Zhang and H. Wang, *Fuel Process. Technol.*, 2023, **242**, 107653.
- 32 M. Norouzi and D. Elhamifar, *Composites, Part B*, 2019, **176**, 107308.
- 33 R. Samiee-Zafarghandi, A. Hadi and J. Karimi-Sabet, *Biomass Bioenergy*, 2019, **121**, 13–21.
- 34 W. Zheng, R. Tan, S. Yin, Y. Zhang, G. Zhao, Y. Chen and D. Yin, *Catal. Sci. Technol.*, 2015, **5**, 2092–2102.
- 35 A. Bahuguna, A. Kumar, T. Chhabra, A. Kumar and V. Krishnan, *ACS Appl. Nano Mater.*, 2018, **1**, 6711–6723.
- 36 D. Pore, K. Undale, B. Dongare and U. Desai, *Catal. Lett.*, 2009, **132**, 104–108.
- 37 S. Abdolahi, M. Hajjami and F. Gholamian, *Res. Chem. Intermed.*, 2021, **47**, 1883–1904.
- 38 M. Esmaeilpour, J. Javidi, F. Dehghani and F. N. Dodeji, *RSC Adv.*, 2015, **5**, 26625–26633.
- 39 A. Khazaei, F. Gholami, V. Khakyzadeh, A. R. Moosavi-Zare and J. Afsar, *RSC Adv.*, 2015, **5**, 14305–14310.
- 40 F. Shahbazi and K. Amani, *Catal. Commun.*, 2014, **55**, 57–64.
- 41 Q. Zhang, Y.-H. Gao, S.-L. Qin and H.-X. Wei, *Catalysts*, 2017, **7**, 351.

